Microscopic mechanism of the tunable band gap in potassium-doped few-layer black phosphorus

Sun-Woo Kim,[1] Hyun Jung,[1] Hyun-Jung Kim,[2] Jin-Ho Choi,[1,3] Su-Huai Wei,[4,*] and Jun-Hyung Cho[1,†]

[1]*Department of Physics and Research Institute for Natural Sciences, Hanyang University, 222 Wangsimni-ro, Seongdong-gu, Seoul 133-791, Korea*

[2]*Korea Institute for Advanced Study, 85 Hoegiro, Dongdaemun-gu, Seoul 130-722, Korea*

[3]*Research Institute of Mechanical Technology, Pusan National University, 2 Pusandaehak-ro 63 beon-gil, Geumjeoung-gu, Korea*

[4]*Beijing Computational Science Research Center, Beijing 100094, China*

(Received 13 June 2017; revised manuscript received 24 July 2017; published 14 August 2017)

Tuning band gaps in two-dimensional (2D) materials is of great interest for the fundamental and practical aspects of contemporary material sciences. Recently, black phosphorus (BP) consisting of stacked layers of phosphorene was experimentally observed to show a widely tunable band gap by means of the deposition of potassium (K) atoms on the surface, thereby allowing great flexibility in the design and optimization of electronic and optoelectronic devices. Here, based on density-functional theory calculations, we demonstrates that the donated electrons from K dopants are mostly localized in the topmost BP layer and this surface charging efficiently screens the K ion potential. It is found that, as the K doping increases, the extreme surface charging and its screening of K atoms shift the conduction bands down in energy, i.e., towards a higher binding energy, because they have more charge near the surface, while it has little influence on the valence bands having more charge in the deeper layers. This result provides a different explanation for the observed tunable band gap compared to the previously proposed giant Stark effect where a vertical electric field from the positively ionized K overlayer to the negatively charged BP layers shifts the conduction band minimum Γ_{1c} (valence band minimum Γ_{8v}) downwards (upwards). The present prediction of Γ_{1c} and Γ_{8v} as a function of the K doping reproduces well the widely tunable band gap, anisotropic Dirac semimetal state, and band-inverted semimetal state, as observed in an angle-resolved photoemission spectroscopy experiment. Our findings shed new light on a route for tunable band gap engineering of 2D materials through the surface doping of alkali metals.

DOI: 10.1103/PhysRevB.96.075416

I. INTRODUCTION

Research on two-dimensional (2D) graphene has attracted enormous interest because of graphene's unique massless Dirac fermionlike electronic structure, which provides a superior carrier mobility for potential applications in electronic devices [1–3]. However, the gapless nature of graphene limits the on-off current ratio in field-effect transistors [4], hindering its utilization in electronic switching technologies. This inherent disadvantage of gapless graphene naturally leads to the development of new field-effect transistors using other 2D materials possessing intermediate band gaps, such as transition-metal dichalcogenides [5–7]. It has been known that the band gaps of semiconducting transition-metal dichalcogenides can be tuned by varying the film thickness [5,6], allowing great flexibility in designing electronic and optical devices.

Similarly, as an elemental 2D material, black phosphorus (BP) also exhibits tunability of the band gap with respect to the film thickness [8–10]. Since monolayer or few-layer BP was successfully fabricated by mechanical exfoliation [8,11], the tunable band gap depending on the film thickness has drawn much attention for its possible application in nanoelectronics [9,10,12]. Especially, monolayer BP has a puckered honeycomb lattice, giving rise to armchair-shaped and zigzag-shaped patterns along the x and y directions, respectively [see Figs. 1(a) and 1(b)]. This anisotropic geometry of monolayer BP results in the interesting anisotropic thermal, optical, and electronic transport properties of few-layer BP [9,12,13]. Moreover, the band gap of monolayer or few-layer BP was found to be highly susceptible to strain and electric field [14–16]. According to the density-functional theory (DFT) calculation of Liu *et al*. [16], an externally applied electric field along the direction normal to the surface of few-layer BP shifts the valence and conduction bands upward and downward, respectively, representing the Stark effect. This electric-field-induced Stark effect was found to produce band inversion of the valence and conduction bands with increasing electric field, leading to a phase transition from a normal insulator to a topological insulator [16] or a Dirac semimetal state [17,18]. Meanwhile, using the deposition of K atoms on the surface of BP, in an angle-resolved photoemission spectroscopy (ARPES) experiment Kim *et al.* [19] observed the widely tunable band gap, an anisotropic Dirac semimetal state with a linear (quadratic) dispersion in the armchair (zigzag) direction, and a band-inverted semimetal state. In order to simulate the low densities of K dopants using the DFT calculation, Kim *et al.* [19] artificially increased the vertical distance d_v between adsorbed K atoms and the four-layer BP surface from the optimized 2×2 structure (containing a single K atom in the 2×2 surface unit cell). From this model calculation, they predicted a variation of the band gap with respect to d_v and argued that the observed tunable band gap was caused by a giant Stark effect induced by a vertical electric field from the positively ionized K overlayer to the negatively charged BP layers. This giant Stark effect in K-doped four-layer BP was treated in the same way as that [16] earlier proposed in four-layer BP under an externally applied

*suhuaiwei@csrc.ac.cn
†chojh@hanyang.ac.kr

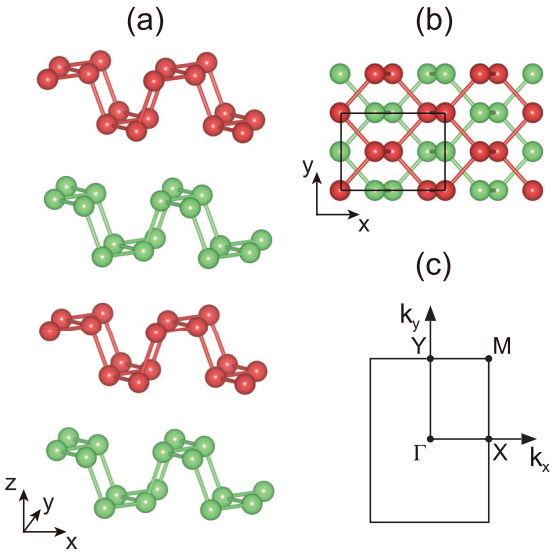

FIG. 1. (a) Side view and (b) top view of the optimized structure of four-layer BP. For distinction, BP layers are alternately drawn with red and green spheres. In (b), the solid line represents the 1×1 unit cell. (c) Surface Brillouin zone.

electric field across the film. However, the present study does not support such an underlying mechanism of the observed tunable band gap, as discussed below.

Here, using first-principles DFT calculations, we investigate not only the adsorption and diffusion of the K atom on the surface of four-layer BP but also the underlying microscopic mechanism of the observed [19] tunable band gap. We find that the K atom adsorbed on the BP surface has an energy barrier of ∼24 meV for diffusion along the zigzag direction, which is much smaller than that (∼353 meV) along the armchair direction. This result indicates the easy (unfeasible) diffusion of K atoms along the zigzag (armchair) direction at the experimental [19] temperature of 15–150 K. Such an anisotropic mobile feature of K atoms on the BP surface is most likely to produce the irregular adsorption patterns in the armchair direction depending on the *in situ* deposition of K atoms in experiments [19]. It is revealed that the donated electrons from K dopants are mostly localized in the topmost BP layer, which can efficiently screen the K ion potential. This extreme surface charging and its screening of K atoms determine the variations of the work function as well as the conduction and valence bands as a function of the dopant density. We obtain two regimes in the variation of the work function with increasing K doping (equivalently, electron doping): i.e., in the initial stage of doping, the work function decreases sharply, while as doping increases further, the function increases slowly. Meanwhile, the conduction band minimum Γ_{1c} decreases monotonously relative to the Fermi level E_F with increasing electron doping, whereas the valence band maximum Γ_{8v} decreases in the first regime but increases in the second regime, consistent with the ARPES data [19]. These variations of Γ_{1c} and Γ_{8v} as a function of the electron doping produce the widely tunable band gap, anisotropic Dirac semimetal state, and band-inverted semimetal state, as observed in ARPES experiments [19]. The present findings provide a new microscopic picture for designing a widely tunable band gap of few-layer BP through the surface deposition of K atoms.

II. COMPUTATIONAL METHODS

Our DFT calculations were performed using the Vienna *ab initio* simulation package (VASP) [20,21] and the all-electron FHI-AIMS code [22]. In the VASP, projector-augmented wave potentials were employed to describe the interaction between ion cores and valence electrons [23]. For treatment of the exchange-correlation energy, we used the generalized-gradient approximation functional of Perdew-Burke-Ernzerhof (PBE) [24]. van der Waals interactions were included using the PBE-D3 scheme [25]. A plane-wave basis was employed with a kinetic energy cutoff of 550 eV, and **k**-space integration was done with a 10×14 mesh in the surface Brillouin zone. The few-layer BP was modeled by a periodic slab geometry consisting of four layers with ∼20 Å of vacuum between the slabs. We employed a dipole correction that cancels the artificial electric field across the slab. All atoms were allowed to relax along the calculated forces until all the residual force components were less than 0.005 eV/Å. For the simulation of electron doping, we used the virtual crystal approximation (VCA) [26] implemented in the FHI-AIMS [22] code to compensate excess electrons by varying the nuclear charge of the P atoms in the BP surface layer, where the donated electrons from K dopants are mostly localized, as discussed below. The employed VCA scheme was successfully applied to electron doping in the In/Si(111) surface system [27].

III. RESULTS

We begin to study the adsorption and diffusion of an isolated K atom on the BP surface using the PBE-D3 scheme. For this, we calculate the potential energy surface (PES) by optimizing the atomic structure of the K adatom within a large 3×3 supercell, which can make negligible the spurious interactions between K adatoms in the neighboring supercells. Figure 2(a) shows a contour plot of the PES, obtained from the 16×8 adsorption sites in a half of the 1×1 unit cell. We find that the K atom prefers to adsorb at the hollow (H) site with a binding energy (E_b) of 1.89 eV. Here, E_b is defined as $E_{\rm tot}({\rm BP}) + E_{\rm tot}({\rm K}) - E_{\rm tot}({\rm K/BP})$, where the first, second, and third terms are the total energies of the clean four-layer BP, the spin-polarized K atom, and the K adsorbed BP system, respectively. We also find that the diffusion energy barrier (D_b) of K is ∼24 meV along the zigzag direction, which is significantly smaller than that (∼353 meV) along the armchair direction. Here, we use the nudged elastic band method [28] to obtain D_b more accurately [see Fig. 2(b)]. Based on these results for the PES and D_b, we estimate that (i) K diffusion is kinetically more facilitated along the zigzag direction than the armchair direction, by a factor of $\sim 10^{11}$ at the experimental temperature of 150 K; and (ii) using an Arrhenius-type activation process with a typical pre-exponential factor of $\sim 10^{13}$ Hz, the K diffusion rate from an H site to a neighboring H site along the zigzag direction amounts to $\sim 8.6 \times 10^4$ ($\sim 1.6 \times 10^{12}$) s^{-1} at 15 (150) K. Therefore, we can say that, at the experimental [19] temperature of 15–150 K, K atoms are

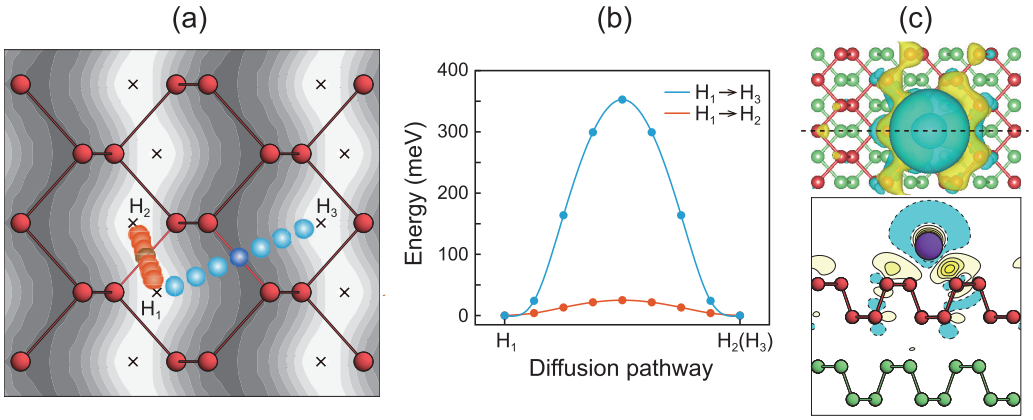

FIG. 2. (a) Calculated PES for an adsorbed K atom on one BP surface. The contour spacing is 0.05 eV, and the energy 0 is set to the H adsorption site (marked with an ×). Minimum-energy diffusion pathways of K along the zigzag ($H_1 \rightarrow H_2$) and armchair ($H_1 \rightarrow H_3$) directions are shown by spheres. Here, the darker circle represents the transition state in each pathway. (b) The corresponding energy profiles. (c) The calculated charge density difference $\Delta\rho$ (defined in the text) is drawn with an isosurface of 0.5×10^{-3} e/Å^3. The contour plot in the vertical plane along the dashed line is also drawn with the first solid or dashed line of $\pm 0.3 \times 10^{-3}$ e/Å^3 and a contour spacing of 1.5×10^{-3} e/Å^3. The solid yellow line represents accumulated electrons; the dashed cyan line, depleted electrons.

restricted to easily diffuse along the zigzag direction, thereby giving rise to evenly distributed K adatoms at the H sites parallel to the zigzag chains. By artificially increasing d_v between the 2 × 2 K overlayer and the four-layer BP surface, Kim *et al.* [19] simulated the relatively weaker electric field at a low dopant density. Since this DFT simulation by Kim *et al.* gave a variation of the band gap E_g ($=\Gamma_{1c} - \Gamma_{8v}$) with respect to d_v, they claimed that a vertical electric field from positively ionized K donors modulates the band gap, owing to the giant Stark effect [19]. However, the present study demonstrates that their prediction of E_g vs d_v is not due to the Stark effect but can be attributed to the screened K ion potential, as discussed below.

Based on the calculated PES in Fig. 2(a), the transverse distribution of K atoms on the BP surface is likely to be determined upon their *in situ* deposition because K adatoms are prevented from diffusing across the zigzag chains at the experimental [19] temperature of 15–150 K. Despite such irregular adsorption patterns of K adatoms, the introduction of electron doping in few-layer BP can be accomplished through charge transfer from K dopants. Indeed, according to ARPES experiments [19], when the anisotropic Dirac band is formed with a band-gap closure, the amount of electron doping was experimentally estimated to be $n_c = 8.3 \times 10^{13}$ cm^{-2}, which is equivalent to ∼0.12 electron (e) per 1 × 1 unit cell [29]. In order to estimate the electron transfer from adsorbed K atom to the BP layers, we calculate the charge density difference, defined as

$$\Delta\rho = \rho_{K/BP} - (\rho_K + \rho_{BP}), \quad (1)$$

where $\rho_{K/BP}$ is the charge density of the equilibrium structure in Fig. 2(a) and $\rho_K + \rho_{BP}$ is the superposition of the charge densities of the separated systems, i.e., the 3×3 K overlayer and the clean BP slab. Figure 2(c) shows that electron charge is transferred mainly from the region on top of the K atom into the region above the neighboring P atoms. It is thus likely that such a strong surface charging of donated electrons easily screens the electric potential of K ions.

To find the variation of E_g with respect to electron doping from K dopants, we calculate the band structure of four-layer BP with increasing excess electronic charge (n) per 1 × 1 unit cell. Such electron doping into four-layer BP is simulated using the VCA [26] without K adatoms on the BP surface. We note, however, that the screened potential of K ions is effectively incorporated in the VCA by increasing the nuclear charge of the P atoms at the BP surface layer. Figures 3(a)–3(d) show the calculated band structures of the clean and electron-doped (n = 0.3 e, 0.37 e, and 0.4 e) four-layer BP, respectively. Here, we use the PBE calculation to obtain the geometry and band structure of each system [30]. We find that the clean four-layer BP has $E_g = 0.37$ eV from the energy difference between Γ_{1c} and Γ_{8v} [see Fig. 3(a)]. This value of E_g is in good agreement with that (0.36 eV) from a previous PBE calculation [31]. It is noted that the Γ_{8v} state has the of the s, p_x, p_y, and p_z orbitals at a ratio of 7%:3%:0%:90%. The most dominant p_z orbital character of Γ_{8v} represents an electron accumulation along the out-of-plane bonds of two P sublayers in the puckered honeycomb lattice [see Fig. 3(a)]. Meanwhile, the Γ_{1c} state has the corresponding partial density of states ratio 18%:26%:0 %:56%, indicating that the sum of s and p_x is comparable in magnitude with p_z. Consequently, contrasting with Γ_{8v}, the charge character of Γ_{1c} shows not only nodes in the out-of-plane bonds but also some electron accumulation in the in-plane bonds within each P sublayer [see Fig. 3(a)].

Figure 3(e) shows that E_g decreases monotonously with increasing n. We find that E_g closes at a critical value of $n_c = 0.37$ e, leading to the formation of a Dirac semimetal with linear and parabolic band dispersions along the Γ-X and Γ-Y lines [see Fig. 3(c)], respectively. It is noted that electron doping changes the characters of Γ_{1c} and Γ_{8v} [see Figs. 3(b) and 3(d)]: i.e., Γ_{1c} exhibits a significant localization at the surface layer, while Γ_{8v} shows some localization below the surface layer. These characters of Γ_{1c} and Γ_{8v} are similar to those obtained under an external electric field applied normal to the surface [16]. Specifically, for $n = 0.4$ e, such charge characters of Γ_{1c} and Γ_{8v} clearly show that the conduction band

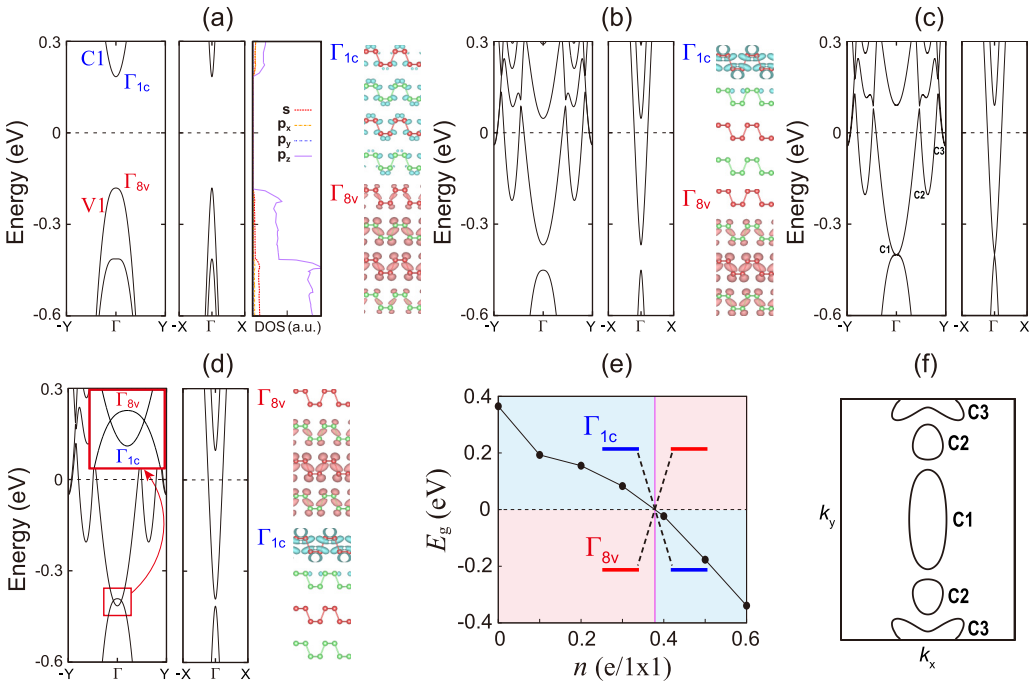

FIG. 3. Calculated band structures of four-layer BP using the VCA (a) without electron doping and (b) with $n = 0.3$, (c) with $n_c = 0.37$ (the Dirac semimetal state), and (d) with $n = 0.4$ e per 1×1 unit cell. Here, Γ_{1c} and Γ_{8v} represent the conduction band (C1) minimum and the valence band (V1) maximum, respectively. The energy 0 is set to the Fermi level. The charge characters of Γ_{1c} and Γ_{8v} are drawn with an isosurface of 0.5×10^{-2} e/Å^3. (e) E_g is displayed as a function of n, where the inversion of the C1 and V1 bands is shown schematically. (f) Calculated Fermi surface of the Dirac semimetal state ($n_c = 0.37$ e) within the surface Brillouin zone.

C1 and the valence band V1 are inverted with each other around the Γ point [see Figs. 3(d) and 3(e)]. This band inversion creates a pair of Dirac points with time-reversal symmetry along the Γ-Y line [see inset in Fig. 3(d)]. These predictions of a widely tunable band gap, anisotropic Dirac semimetal state, and band-inverted semimetal state with increasing n are consistent with ARPES measurements [19]. Although the present simulation does not take into account the electric field by excluding the presence of K adatoms above the surface, our results imply that the previously proposed [19] giant Stark effect is not the main cause for the observed tunable band gap.

It is interesting to understand how the surface charging achieved with electron doping from K dopants produces the variation of E_g. For this, we plot in Fig. 4(a) the Fermi level E_F and the binding energy $E_{\Gamma_{1c}}$ ($E_{\Gamma_{8v}}$) of Γ_{1c} (Γ_{8v}) as a function of n, relative to the vacuum level. It is shown that E_F increases sharply at the initial stage of doping between $0 \leqslant n < \sim 0.2$ e, but it decreases slowly when $n \geqslant \sim 0.2$ e, giving rise to an initial decrease and a subsequent increase in the work function in the first and second regimes, respectively. Here, the upward shift of E_F in the first regime is due to the initial occupation of the C1 band, while the downward shift in the second regime is mostly attributed to the significant lowering of the C1 band [see Fig. 3(b)]. Interestingly, it is shown in Fig. 4(a) that, in the first regime, Γ_{1c} varies slightly relative to the vacuum level, but it decreases sharply in the second regime. On the other hand, in the first regime, Γ_{8v} shifts upward by 0.24 eV from the value obtained without electron doping, while it is nearly unchanged in the second regime [see Fig. 4(a)]. These contrasts of Γ_{1c} and Γ_{8v} under electron doping can be associated with the effect of the screened K ion potential due to surface charging, i.e., Γ_{1c}, possessing a localized charge character at the surface, shifts toward a high binding energy as n increases, whereas Γ_{8v}, with a scarce surface charge, is nearly insensitive with increasing n.

In Fig. 4(b), the variation of $E_{\Gamma_{1c}}$ and $E_{\Gamma_{8v}}$ relative to E_F is again plotted as a function of n. It is seen that Γ_{1c} decreases monotonously with increasing n, while Γ_{8v} initially decreases but subsequently increases. Overall, these variation patterns of Γ_{1c} and Γ_{8v} are consistent with the ARPES data [19], which exhibit a monotonously downward shift of Γ_{1c} and an initially downward but subsequently upward shift of Γ_{8v} [see Fig. 4(c)]. Specifically, it is seen that, when $n \geqslant \sim 0.2$ e, Γ_{1c} and Γ_{8v} are progressively closer to each other and eventually cross at $n_c = 0.37$ e. These downward and upward shifts of Γ_{1c} and Γ_{8v} with increasing n were previously [19] explained by the giant Stark effect, which could be induced by the electric field from the positively ionized K atoms to the negatively charged BP layers. However, we here demonstrate that the upward shift of Γ_{8v} is attributed to the above-mentioned lowering of E_F for $n \geqslant \sim 0.2$ e [see Fig. 4(a)], which is induced by the significant shift of Γ_{1c} toward a high binding energy due to the efficient screening of the K ion potential at the surface. We note that, if the electric field generated by the K overlayer is associated with the opposite shifts of Γ_{1c} and Γ_{8v}, the adsorption of K atoms on both sides of the four-layer BP slab would not influence E_g because their created electric fields should cancel each other. However, our PBE calculation

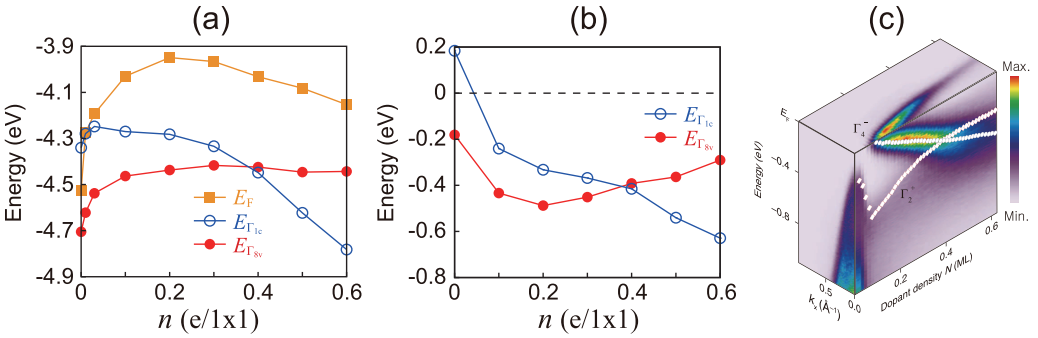

FIG. 4. (a) Calculated E_F, $E_{\Gamma_{1c}}$, and $E_{\Gamma_{8v}}$ relative to the vacuum level, as a function of n. (b) $E_{\Gamma_{1c}}$ and $E_{\Gamma_{8v}}$ relative to E_F. (c) ARPES data for the evolution of Γ_{1c} (Γ_4^-) and Γ_{8v} (Γ_2^+) as a function of the K dopant density are taken from Ref. [19]. Reprinted with permission from AAAS. Here, blue circles and red diamonds denote $E_{\Gamma_{1c}}$ and $E_{\Gamma_{8v}}$ relative to E_F, respectively.

for such a structure of K adsorption with inversion symmetry shows that E_g still varies with increasing d_v (see Fig. 5), similar to the previous result [19] obtained in the case of K adsorption on one side of the BP slab. Moreover, despite the fact that the *in situ* deposition of a certain number of K atoms could yield irregular adsorption patterns in experiments (as discussed above), the ARPES data [19] showed an invariance of the tunable band gap as a function of the dopant density [19]. This also implies that the electric field from the K adatoms to the BP layers would not play a major role in tuning E_g. Thus, the previously proposed giant Stark effect [19] is probably not the origin of the observed tunable band gap in K-doped few-layer BP.

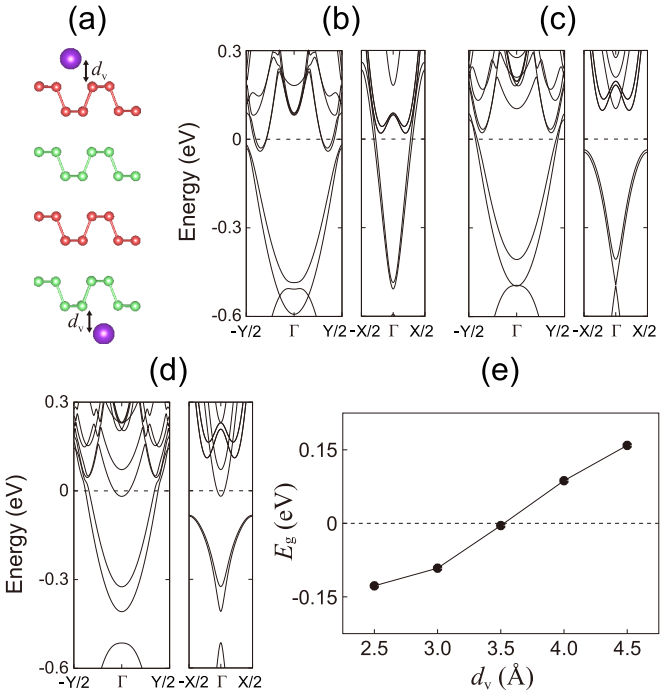

FIG. 5. (a) Optimized 2×2 structure with K atoms on both sides of the four-layer BP slab and its band structures at (b) $d_v = 2.5$ Å (the equilibrium state), (c) $d_v = 3.5$ Å, and (d) $d_v = 4.5$ Å. The energy 0 is set to the Fermi level. In (e), E_g is displayed as a function of d_v.

It is noteworthy that, although the present study captures essential features of how E_g is tuned via surface charging and its screening of K atoms, the predicted value of $n_c = 0.37$ e is much larger than that ($n_c = 0.12$ e) estimated from ARPES experiments [19,29]. For this discrepancy, we discuss some reasons from the experimental and theoretical points of view. First, Kim *et al.* [19] may underestimate the value of n_c, because they estimated the electron concentration by taking into account only the area of the C1 band enclosed by the Fermi surface using Luttinger's theorem [32]. However, according to our band structure obtained at n_c, the Fermi surface encircles not only the C1 band around the Γ point but also the C2 or C3 band along the positive and negative Γ-Y directions [see Figs. 3(c) and 3(f)]. Here, we obtain the ratio of their areas as C1:C2:C3 = 44.6%:24.6%:30.8%. Using this ratio, we estimate that the experimental value of n_c can be increased to ∼0.27 e. Moreover, the effective mass is not a constant as Luttinger's theorem assumes, but it increases as the electron filling increases, which further increases n_c. It is noted that the series of ARPES intensity maps at constant energies showed strong suppression along the Γ-Y direction with respect to the Γ-X direction. Therefore, it is quite likely that the ARPES experiment of Kim *et al.* [19] could not detect the presence of the C2 and C3 bands. Second, unlike the experimental condition of rather thick BP samples [19], the four-layer BP slab employed in the present theoretical simulation with the PBE functional may induce some overestimation of n_c. It is noted that doping-induced band renormalization can also contribute to the band-gap reduction [33,34]. Also, the presently employed VCA for electron doping may not accurately describe the screened K ion potential. In these respects, more refined experimental and theoretical works are anticipated in future to reduce the quantitative difference in n_c between the previous ARPES experiment [19] and the present theory.

IV. SUMMARY

We have performed a first-principles DFT study to explore the underlying mechanism of the observed tunable band gap in K-doped few-layer BP. Unlike the previously proposed giant Stark effect [19], we demonstrated that the variation of E_g as a function of the dopant density is caused by the ionic

potential of K and the extreme surface charging of donated electrons and its screening of the K ion potential. It was found that, as electron doping increases, Γ_{1c} monotonously decreases relative to the Fermi level, while Γ_{8v} decreases in the initial stage of doping but increases subsequently. Consequently, we reproduced the widely tunable band gap, anisotropic Dirac semimetal state, and band-inverted semimetal state, in good agreement with the ARPES measurements [19]. The present findings offer a new aspect for designing a tunable band gap in 2D materials via surface charging with alkali-metal dopants.

ACKNOWLEDGMENTS

This work was supported by National Research Foundation of Korea (NRF) grants funded by the Korean Government (Grants No. 2015M3D1A1070639 and No. 2015R1A2A2A01003248). S.W. is supported by the NSFC (Grant No. U1530401). Calculations were performed by the KISTI supercomputing center through the strategic support program (KSC-2016-C3-0059) for supercomputing application research. S.W.K. acknowledges support from POSCO TJ Park Foundation.

[1] K. S. Novoselov, A. K. Geim, S. V. Morozov, D. Jiang, Y. Zhang, S. V. Dubonos, I. V. Grigorieva, and A. A. Firsov, Science **306**, 666 (2004).
[2] K. S. Novoselov, A. K. Geim, S. V. Morozov, D. Jiang, M. I. Katsnelson, I. V. Grigorieva, S. V. Dubonos, and A. A. Firsov, Nature **438**, 197 (2005).
[3] Y. Zhang, J. W. Tan, H. L. Stormer, and P. Kim, Nature **438**, 201 (2005).
[4] F. Xia, D. B. Farmer, Y.-M. Lin, and P. Avouris, Nano Lett. **10**, 715 (2010).
[5] Q. H. Wang, K. Kalantar-Zadeh, A. Kis, J. N. Coleman, and M. S. Strano, Nat. Nanotechnol. **7**, 699 (2012).
[6] X. Duan, C. Wang, A. Pan, R. Yu, and X. Duan, Chem. Soc. Rev. **44**, 8859 (2015).
[7] C. Tan and H. Zhang, Chem. Soc. Rev. **44**, 2713 (2015).
[8] H. Liu, A. T. Neal, Z. Zhu, Z. Luo, X. Xu, D. Tománek, and P. D. Ye, ACS Nano **8**, 4033 (2014).
[9] L. Kou, C. Chen, and S. C. Smith, J. Phys. Chem. Lett. **6**, 2794 (2015).
[10] L. Li, J. Kim, C. Jin, G. J. Ye, D. Y. Qiu, F. H. da Jornada, Z. Shi, L. Chen, Z. Zhang, F. Yang, K. Watanabe, T. Taniguchi, W. Ren, S. G. Louie, X. H. Chen, Y. Zhang, and F. Wang, Nat. Nanotechnol. **12**, 21 (2017).
[11] L. Li, Y. Yu, G. J. Ye, Q. Ge, X. Ou, H. Wu, D. Feng, X. H. Chen, and Y. Zhang, Nat. Nanotechnol. **9**, 372 (2014).
[12] X. Ling, H. Wang, S. Huang, F. Xia, and M. S. Dresselhaus, Proc. Natl. Acad. Sci. USA **112**, 4523 (2015).
[13] Z. Li, T. Cao, M. Wu, and S. G. Louie, Nano Lett. **17**, 2280 (2017).
[14] R. Fei and L. Yang, Nano Lett. **14**, 2884 (2014).
[15] A. S. Rodin, A. Carvalho, and A. H. Castro Neto, Phys. Rev. Lett. **112**, 176801 (2014).
[16] Q. Liu, X. Zhang, L. B. Abdalla, A. Fazzio, and A. Zunger, Nano Lett. **15**, 1222 (2015).
[17] S. S. Baik, K. S. Kim, Y. Yi, and H. J. Choi, Nano Lett. **15**, 7788 (2015).
[18] J. Ahn and B.-J. Yang, Phys. Rev. Lett. **118**, 156401 (2017).
[19] J. Kim, S. S. Baik, S. H. Ryu, Y. Sohn, S. Park, B.-G. Park, J. Denlinger, Y. Yi, H. J. Choi, and K. S. Kim, Science **349**, 723 (2015).
[20] G. Kresse and J. Hafner, Phys. Rev. B **48**, 13115 (1993).
[21] G. Kresse and J. Furthmüller, Comput. Mater. Sci. **6**, 15 (1996).
[22] V. Blum, R. Gehrke, F. Hanke, P. Havu, V. Havu, X. Ren, K. Reuter, and M. Scheffler, Comput. Phys. Commun. **180**, 2175 (2009).
[23] G. Kresse and D. Joubert, Phys. Rev. B **59**, 1758 (1999).
[24] J. P. Perdew, K. Burke, and M. Ernzerhof, Phys. Rev. Lett. **77**, 3865 (1996).
[25] S. Grimme, J. Antony, S. Ehrlich, and H. Krieg, J. Chem. Phys. **132**, 154104 (2010).
[26] N. A. Richter, S. Sicolo, S. V. Levchenko, J. Sauer, and M. Scheffler, Phys. Rev. Lett. **111**, 045502 (2013).
[27] S.-W. Kim, H.-J. Kim, F. Ming, Y. Jia, C. Zeng, J.-H. Cho, and Z. Zhang, Phys. Rev. B **91**, 174434 (2015).
[28] G. Henkelman, B. P. Uberuaga, and H. Jónsson, J. Chem. Phys. **113**, 9901 (2000).
[29] Using Luttinger's theorem, Kim *et al.* [19] estimated n_c as $\sim 8.3 \times 10^{13}$ cm^{-2}. Considering that the area of the 1×1 unit cell is 1.48×10^{-15} cm^2 in the present DFT calculation, this experimental value of n_c is equivalent to ~ 0.12 e per 1×1 unit cell. It is noted that this amount of heavy carrier doping in BP can be achieved in gated devices or by ionic liquid gating [see Y. Saito and Y. Iwasa, ACS Nano **9**, 3192 (2015)]. Therefore, by inducing the ultrahigh carrier density of $\sim 10^{13}$/cm^2, BP field-effect transistors may be realized to control high mobility and current modulations.
[30] Using the PBE-D3 calculation, we obtained $E_g = 0.09$ eV for a clean four-layer BP, in good agreement with that (0.07 eV) from a previous PBE-D2 calculation [16]. Since this value of E_g is largely underestimated compared to that (~ 0.3 eV) measured in ARPES experiments [19], we performed the PBE calculation which properly predicted the magnitude of E_g.
[31] J. Qiao, X. Kong, Z.-X. Hu, F. Yang, and W. Ji, Nat. Commun. **5**, 4475 (2014).
[32] J. M. Luttinger, Phys. Rev. **119**, 1153 (1960).
[33] Y. Liang and L. Yang, Phys. Rev. Lett. **114**, 063001 (2015).
[34] A. Walsh, J. L. F. Da Silva, and S.-H. Wei, Phys. Rev. B **78**, 075211 (2008).